Nanopore Formation in a Polyphenylene Low-k Dielectric

Michael S. Silverstein[1], Barry J. Bauer[2], Ronald C. Hedden[3], Hae-Jeong Lee[2] and Brian G. Landes[4]

[1]*Department of Materials Engineering, Technion – Israel Institute of Technology, Haifa 32000, Israel*

[2]*Polymers Division, National Institute of Standards and Technology, Gaithersburg, MD 20899, USA*

[3]*Department of Materials Science and Engineering, Penn State University, University Park, PA 16802, USA*

[4]*Dow Chemical Company, Midland, MI 48674, USA*

INTRODUCTION

The demand for increased signal transmission speed and device density in the next generation of multilevel integrated circuits has placed stringent demands on materials performance. Nanometer-scale porosity is being introduced into low-k dielectrics in an attempt to achieve such low permittivities. To facilitate development of low-k materials with optimal properties, the pore structure must be characterized. However, it has proved extremely difficult to describe the mechanism of pore formation and to characterize the porous structure (porosity, pore size, pore size distribution) owing to the nanometer scale of the pores. The combination of x-ray reflectivity (XRR) and small angle neutron scattering (SANS) has been demonstrated to be a powerful technique for describing the porosity and nanoscale architecture of nanoporous low-k thin films.[1-4] This work investigates pore formation in a polyphenylene low-k dielectric based on pyrolysis of a porogen in a polyphenylene oligomer matrix.[5] One unique aspect of this research is the description of the nanoscale structure at various stages of pore formation through the use of a deuterated porogen.

EXPERIMENTAL

Certain commercial equipment and materials are identified in this paper in order to specify adequately the experimental procedure. In no case does such identification imply recommendation by NIST nor does it imply that the material or equipment identified is necessarily the best available for this purpose.

Materials. The porous organic low-k material investigated in this research is based on a developmental version (V7) of Dow Chemical's SiLK polyphenylene precursor especially prepared for this work. The deuterated polymeric porogen (hereafter referred to as the porogen) yields neutron scattering contrast in the porogen-oligomer system. The densities of the low-k crosslinked polymeric matrix (the oligomer following a complete cure, hereafter referred to as the polymer) and the porogen are (1.18 and 1.07) g/cm^3, respectively. The oligomer to porogen mass ratio was 75:25.

The films were prepared by spin-casting a porogen-filled oligomer and subsequently baking at 150 °C. Two sets of samples were prepared; Set A was baked at 150 °C for 24 h, while Set B was baked at 150 °C for 48 h. Films at various stages of porogen degradation were investigated. Previous experience with the thermal degradation of the porogen indicates that porogen degradation is incomplete following a cure at 400 °C, while porogen degradation is complete following a cure at 430 °C. The films were not held at the cure temperature except for specific samples held for 40 min at 430 °C. The sample names reflect the maximum processing temperature followed by the cure hold time in minutes (if applicable) and the bake process (A or B) (e.g. 43040A: 430 °C, 40 min, Set A).

X-Ray Reflectivity. Specular x-ray reflectivity measurements (XRR) were performed using a modified Philips high-resolution x-ray diffractometer equipped with an environmental control chamber with Be windows. Data were collected at the specular condition, with the grazing incident angle, θ_i, equal to the detector angle θ_d. The reflected intensity was recorded as a function of angle. XRR measurements were performed under vacuum. The magnitude of the x-ray momentum transfer in the film thickness direction, q_z, is related to θ_i and the wavelength of the Cu $K_{\alpha 1}$ radiation (1.54 Å), λ_X, by $q_z = (4\pi \sin\theta_i) / \lambda_X$. The data were plotted as the log of the relative intensity (reflected beam intensity, I, divided by the incident beam intensity, I_0) versus q_z. The average electron densities of the films were deduced using a computer modeling routine (*mlayer*) capable of simulating reflectivity from multi-layer structures.[6]

Small Angle Neutron Scattering. The homogeneous materials in this work, the oligomer, polymer and porogen, can each be described by a neutron scattering length density (SLD). The SLD of component i is $\rho_i\sigma_i$, where ρ_i is its mass density and σ_i is the total scattering length per unit mass defined by:[7]

$$\sigma_i = \sum_j c_j b_j \Big/ \sum_j c_j (m_j / N_A) \qquad \text{Equation 1}$$

where c_j is the local molar concentration of a nucleus j, b_j is its scattering length, m_j is its molar mass, and N_A is Avogadro's number. The densities and compositions were used to calculate the neutron scattering length densities (the oligomer density was assumed to be identical to that of the polymer, 1.18 g/cm^3). The resulting SLD were 2.37 x 10^{-6} Å^{-2} for the oligomer and polymer and 5.67 x 10^{-6} Å^{-2} for the porogen. The scattering contrast between two materials is defined as the difference between their SLD. The porogen-oligomer contrast is therefore 3.30 x 10^{-6} Å^{-2}, greater than the polymer-pore contrast of 2.37 x 10^{-6} Å^{-2}. For a two phase blend in which each phase has a homogeneous atomic composition, the scattered intensity, $I(q)$, is proportional to the contrast between the two phases squared, regardless of sample morphology:

$$I(q) \propto (\rho_1\sigma_1 - \rho_2\sigma_2)^2 \qquad \text{Equation 2}$$

where q is the scattering vector, related to the scattering angle, $2\theta_s$, and the neutron wavelength, λ_N, by $q = (4\pi \sin\theta_s) / \lambda_N$. SANS was performed on the 8 m NG1 instrument, with a wavelength spread of 12 % at the National Institute of Standards and Technology (NIST) Center for Neutron Research using a wavelength of 12 Å. The data are plotted as intensity versus q on a log-log scale. Fits of the scattering data were made by a least squares fit, giving an average and a standard deviation to the fit.

The relative uncertainties of the data presented are estimated as one standard deviation of the mean. The total combined uncertainties from all external sources are not reported, as comparisons are made with data obtained under the same conditions. In cases where the limits are smaller than the plotted symbols, the limits are left out for clarity. All temperatures reported are within ± 1 °C, thicknesses are within ± 1 nm, q_c^2 within ± 1 X10^{-5} Å^{-1}, and densities and porosities within ± 3 %, as determined by previous experience of repeated measurements. The standard deviations from the fits of the SANS data using a polydisperse hard sphere model were less than: ± 2 % for radius, ± 3 % for polydispersity and ± 0.5 % for scattering contrast.

RESULTS AND DISCUSSION

X-Ray Reflectivity. XRR profiles in vacuum for the porogen-filled oligomer (150A), for incomplete porogen degradation (400A) and for complete porogen degradation (43040A) are shown in Figure 1. The critical edge, q_c, which is the q_z value at the sharp drop in log (I/I_0) from the initially flat reflectivity curve, is quite clear in each case. The data were fit to find q_c^2, which was then used to calculate the electron density. For the materials with a known atomic composition (150, 430, 43040), the electron density was used to calculate the effective mass density, d_{eff} ((1.120 and 1.019) g/cm^3 for 150A and 43040A, respectively).[1,2] The porosity, p_V, for 43040A calculated using Equation 3 (mass balance), is 13.6%.

$$d_{eff} = d(1 - p_v) \qquad \text{Equation 3}$$

where d is the density of the dense (non-porous) wall material. The porosities of the samples cured at 400 °C could not be determined using XRR in vacuum since their molecular structures and wall densities are unknown. However, the porosities of such samples can be determined by XRR after filling the pores with a known solvent.

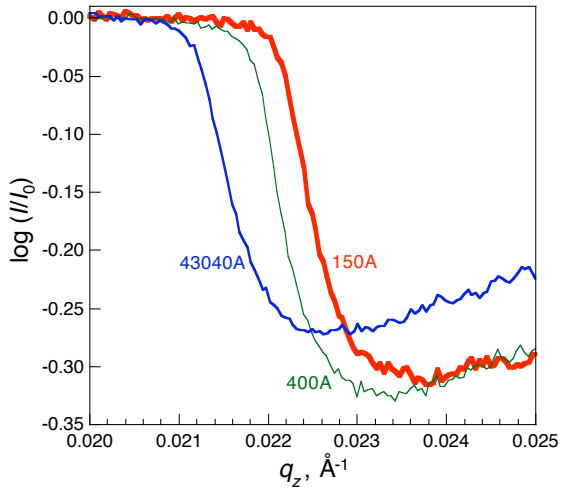

Figure 1. XRR in vacuum for various cure temperatures.

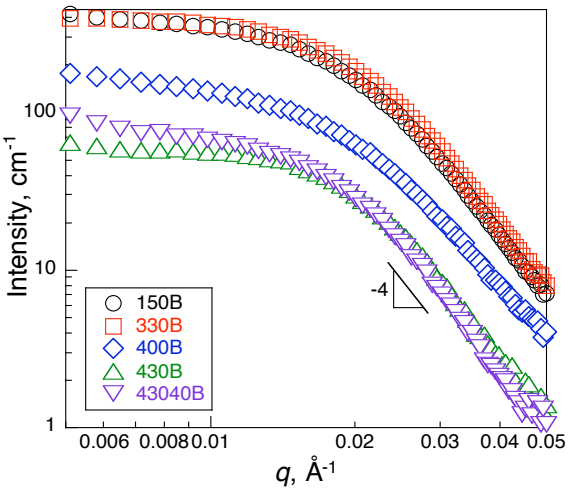

Figure 2. SANS for various cure temperatures.

The critical edge (Figure 1) decreases with increasing processing temperature, indicating a decrease in film density. The effective density of 150A is 1.12 g/cm^3, close to the density of 1.15 g/cm^3 that was calculated by assuming a density of 1.18 g/cm^3 for the oligomer. Conversely, the measured d_{eff} for 150A and the known molecular structure and porogen density can be used to calculate the density of the oligomer (1.14 g/cm^3) and recalculate the volume content of porogen (26 %). The calculated shrinkage during the cure of a 1.14 g/cm^3 oligomer to a 1.18 g/cm^3 dense (non-porous) polymer is only 3 % (assuming a negligible mass loss during the curing process).

Small Angle Neutron Scattering. The SANS data for all the materials in Set B are presented in Figure 2. All the SANS curves from Set B and all the SANS curves from Set A, except 430A, have similar shapes. The scattering intensities exhibit a plateau below q = 0.01 Å^{-1} and q^{-4} scaling behavior above q = 0.02 Å^{-1}. The similarities in the SANS curves indicates that the two phase structure of the porogen-filled oligomer is similar to the two phase structure of the porous polymer. The scattering intensity in Figure 2 progressively decreases, from that for the uncured material (150B and 330B), to that for the material cured at 400 °C, to that for the material cured at 430 °C (430B and 43040B). There are two reasons for the decrease in the scattering intensity. The scattering contrast between the deuterated porogen and the matrix (150B) is greater than that between the pores and the matrix (430B). The amount of porogen in the system decreases with the increase in curing temperature and this reduction in contrast correspondingly reduces the scattering intensity. In addition, scattering intensity decreases due to the reduction in the (pore/porogen) volume fraction during curing from approximately 26% porogen in the oligomer to approximately 12% pores in the polymer.

The pore size was estimated by fitting the mid-range data to a structural model describing the scattered intensity from a population of polydisperse hard spheres.[8,9] The polydisperse hard sphere (PHS) model includes hard sphere interactions between the particles and uses a Schultz distribution to describe the polydispersity of the radii. The PHS model incorporates five fitting parameters, four of which are independent: mean pore radius R, polydispersity PD (PD = s/R, where s^2 is the variance of the distribution), volume fraction of a second phase v_2 (the porogen, prior to pyrolysis or the pores, following pyrolysis), scattering contrast SC, and background scattering intensity B (taken from the experimental data's q-independent scattering intensity value at high q). SC and v_2, are the dependent parameters. A fixed v_2 of 0.26 was used for the porogen-oligomer system and a fixed v_2 of 0.12 was used for the materials exposed to 430 °C. The porogen domains have a smaller average radius and a wider polydispersity while the pores have a larger average radius and a narrower polydispersity (Table 1).

Table 1. Results from PHS Fits to the SANS Data Using a Fixed v_2

Sample	R, Å (Fit)	PD (Fit)	v_2 (Fixed)	SC, Å^{-2} x 10^6 (Fit)	B, cm^{-1} (Fixed)
150B	64	0.57	0.26	2.5	0.40
330B	77	0.45	0.26	2.7	0.30
430B	85	0.29	0.1	1.4	0.35
43040B	70	0.46	0.12	1.3	0.25

CONCLUSIONS

The combination of XRR and SANS is a powerful tool for describing porogen degradation and pore formation in nanoporous materials. Insight into the pore formation process was obtained through the use of a deuterated porogen and interpreting the SANS data using the PHS model.

ACKNOWLEDGEMENTS

The authors gratefully acknowledge the assistance of Derek L. Ho and Charles J. Glinka, Center for Neutron Research, National Institute of Standards and Technology and the support of the National Institute of Standards and Technology, US Department of Commerce, in providing the neutron research facilities used in this work.

REFERENCES

1. Silverstein, M. S.; Shach-Caplan, M.; Bauer, B. J.; Hedden R. C.; Lee H.-J.; Landes, B. G. *Macromolecules* **2005**, *38*, 4301.
2. Silverstein, M. S.; Bauer, B. J.; Lee, H. J.; Hedden, R. C.; Landes, B.; Lyons, J.; Kern, B.; Niu, J.; Kalantar, T. In *Characterization and Metrology for ULSI Technology 2003, AIP Conference Proceedings*; Seiler, D. G., Diebold, A. C., Shaffner, T. J., McDonald, R., Zollner, S., Khosla, R. P., Secula, E. M., Eds.; AIP: New York, 2003; Vol. 683, p 572.
3. Lee, H. J.; Soles, C. L.; Liu, D. W.; Bauer, B. J.; Wu, W. L. *J. Polym. Sci. B: Polym. Phys.* **2002**, *40*, 2170.
4. Lee, H. J.; Soles, C. L.; Liu, D. W.; Bauer, B. J.; Wu, W. L. *Polymeric Materials: Science and Engineering* **2002**, *87*, 435.
5. Strittmatter, R. J.; Hahnfeld, J. L.; Silvis, H. C.; Stokich, T. M.; Perry, J. D.; Ouellette, K. B.; Niu, Q. J.; Godschalx, J. P.; Kalantar, T. H.; Mubarekyan, E.; Hefner, R. E.; Lyons, J. W.; Dominowski J. M.; Buske, G. R. *Mat. Res. Soc. Symp. Proc.* **2003**, *766*, E7.5.1.
6. Ankner, J. F.; Majkrzak, C. F. In *Neutron Optical Devices and Applications, SPIE Conference Proceedings*, Majkrzak, C. F., Wood J. M. Eds.; SPIE, Bellingham, WA, 1992; Vol. 1738, p 261.
7. Hedden, R. C.; Lee, H. J.; Bauer, B. *Langmiur*, **2004**, *20*, 416.
8. Griffith, W. L.; Triolo, R.; Compere, A. L. *Physical Review A* **1986**, *33*, 2197.
9. Griffith, W. L.; Triolo, R.; Compere, A. L. *Physical Review A* **1987**, *35*, 2200.